INTECH OPEN ACCESS PUBLISHER

Magnetic Au Nanoparticles on Archaeal S-Layer Ghosts as Templates

Regular Paper

Sonja Selenska-Pobell[1,*], Thomas Reitz[1], Rico Schönemann[2], Thomas Herrmansdörfer[2], Mohamed Merroun[3], Andrea Geißler[1], Juan Bartolomé[4], Fernando Bartolomé[4], Luis Miguel García[4], Fabrice Wilhelm[5] and Andrei Rogalev[5]

1 Institute of Radiochemistry, Helmholz- Zentrum Dresden-Rossendorf, Germany
2 Dresden High Magnetic Field Laboratory, Helmholz- Zentrum Dresden-Rossendorf, Germany
3 Department of Microbiology, University of Granada, Spain
4 ICMA, Departamento de Física de la Materia Condensada, CSIC ‡ Universidad of Zaragoza, Spain
5 European Synchrotron Radiation Facility (ESRF), France
*Corresponding author E-mail: s.selenska-pobell@hzdr.de

Abstract Cell-ghosts representing empty cells of the archaeon *Sulfolobus acidocaldarius,* consisting only of their highly ordered and unusually stable outermost proteinaceous surface layer (S-layer), were used as templates for Au nanoparticles fabrication. The properties of these archaeal Au nanoparticles differ significantly from those produced earlier by us onto bacterial S-layer sheets. The archaeal Au nanoparticles, with a size of about 2.5 nm, consist exclusively of metallic Au(0), while those produced on the bacterial S-layer had a size of about 4 nm and represented a mixture of Au(0) and Au(III) in the ratio of 40 to 60 %.

The most impressive feature of the archaeal Au nanoparticles is that they are strongly paramagnetic, in contrast to the bacterial ones and also to bulk gold. SQUID magnetometry and XMCD measurements demonstrated that the archaeal Au nanoparticles possess a rather large magnetic moment of about $0.1\mu_B$/atom. HR-TEM-EDX analysis revealed that the archaeal Au nanoparticles are linked to the sulfur atoms of the thiol groups of the amino acid cysteine, characteristic only for archaeal S-layers. This is the first study demonstrating the formation of such unusually strong magnetic Au nanoparticles on a non-modified archaeal S-layer.

Keywords Magnetic Au nanoparticles, archaeal S-layer, High Resolution Transmission Electron Microscopy (HR-TEM, X-ray Magnetic Circular Dichroism (XMCD)

1. Introduction

During the last decade, the production, characterization, and application of nano-sized particles of noble metals have become a fast developing topic of modern science and technology. These particles are an effective bridge between bulk materials and atomic structures and are very perspective for the development of future key technologies. Whereas the bulk materials usually exhibit constant physical properties regardless to their size, the properties of nano-scaled particles are often unusual and dependent on their size and shape mostly due to the dramatically increased number of surface atoms in comparison to their volume [1,2,3]. Nano-sized noble metal particles can be used in catalysis [4,5], biomedicine

[6], as well as optical bio- and chemosensors [7,8]. Along with the large variety of abiotic templates used for the production of metallic nanoparticles, biological substrates are of increasing interest. The biological substrates are advantageous as they provide a non-toxic and therefore environmentally friendly matrix for fabrication of metallic nano-structures. The highly ordered proteinaceous paracrystalline surface layers (S-layers) of some bacteria were used as matrices for production of platinum, palladium, and gold nanoparticles without any chemical modifications [9,10,11,12,13]. Some of these bio-nanoparticles such as bio-Pd, for instance, possess high catalytic capability and exhibit magnetic properties [4,13]. Up-to-date magnetic gold nanoparticles were synthesized exclusively chemically and stabilized by polymers [1]. In some cases the gold nanoparticles were capped by thiol groups to induce ferromagnetism [14]. Interestingly, the S-layer of *B. sphaericus* CCM2177 was modified by thiolysation in order to stimulate the binding of gold [15]. The authors were able to produce Au nanoparticles with a size of 5 nm on this chemically modified bacterial S-layer. However, they did not report magnetic properties of these Au nanoparticles. On the other hand, in our recent studies we have demonstrated that the S-layer of *B. sphaericus* JG-A12, which is closely related to *B. sphaericus* CCM2177 (both strains were reclassified recently to *Lysinobacillus sphaericus* and contain thiol-free S-layers), can be successfully used as a template for Au nanoclusters fabrication without incorporation of thiol groups [11,12].

In the present work, the S-layer protein, called SlaA [16], of the acidothermophilic crenarchaeon *Sulfolobus acidocaldarius* was used as a matrix for the synthesis and stabilization of Au nanoparticles. The rationale for choosing this archaeal S-layer was, on one hand, the indigenous presence of two sulfur-containing cysteine residues per protein monomer [17]. These residues provide thiol groups which can stimulate the binding of Au(III) and the efficacy of the nanoclusters formation. On the other hand, as mentioned above, the presence of thiol groups in the Au nanoclusters may influence their magnetic properties. The archaeal SlaA-layer possesses p3-symmetry and exhibits extreme stability to high acidity and temperatures as well as to proteases and detergents [17,18,19]. The latter property allows the isolation of empty SlaA-layer ghosts, with the shape of the cells, by using standard purification procedures [17, 19]. These ghosts can be mechanically disrupted *via* sonication in monolayer SlaA-layer sheets, which are comparable to those obtained usually from bacteria [19]. It was demonstrated that metals bind to the inner, facing the cells, side of the S-layers [4,20] which is negatively charged [21]. In the case of *S. acidocaldarius* this means that Au(III) should be deposited and reduced inside the thiol containing SlaA-ghosts. This process seems advantageous for Au(0) nanoclusters

formation in comparison to the previously described procedure when monolayers of thiol-free bacterial S-layer sheets were used.

2. Material and methods

2.1 Preparation of the SlaA-layer ghosts

S. acidocaldarius DSM 639 was purchased from DSMZ (Deutsche Sammlung für Mikroorganismen und Zellkulturen), Braunschweig, Germany. It was grown in a 70 L bioreactor (Applikon Biotechnology Inc., Foster City, CA, USA) at pH 2.7 and 70 °C with automatic control of pH, temperature, and dissolved oxygen. The archaeal cells were harvested at the end of the logarithmic growth phase (OD_{600} ~0.9) by centrifugation for 15 min at 10.000 g using continuous flow centrifuge (CARR® ViaFuge® Pilot 9010, Kendro, Newtown, CT, USA).

The cells lysis was performed in 10 mM HEPES buffer (pH 7), containing 2 mM EDTA and 0.15% SDS under stirring for one hour at room temperature, as described in [22]. In order to achieve complete removal of the cytoplasma membrane and the anchored in it SlaB protein [16], the cell lysate was treated with 2% SDS and stirred overnight. Subsequently the suspension was centrifuged for 30 min at 40.000 g. Afterwards, only the upper white part of the pellet was resuspended in HEPES buffer (pH 7) containing 2 mM EDTA and 2% SDS and incubated for one hour at 60 °C. This washing procedure with hot SDS was performed twice. After the last centrifugation, the upper white part of the resulting pellet, consisting of the purified outermost S-layer sacculi, i.e. SlaA-ghosts, was resuspended in distilled water (pH 6.4). SDS was removed from the SlaA-ghosts by eight washing steps with distilled water.

2.2 Morphological and biochemical analyses of the SlaA-ghosts

The shape of the SlaA-ghosts and their purity from non-lysed cells and cell debris are checked by light microscopy at 1000-fold magnification in phase contrast mode (Olympus BX-61, Olympus Optical Co. GmbH, Hamburg, Germany). The presence of other proteins in the SlaA-ghosts fraction was excluded by denaturing sodium dodecyl sulfate polyacrylamide gel electrophoresis (SDS-PAGE) according to [23] in a Mini-PROTEAN® II electrophoresis cell system (Bio-Rad Laboratories, Munich, Germany). For complete dissociation and solubilization, the SlaA-ghosts were initially incubated for 20 min at 45 °C in sodium carbonate buffer (20 mM, pH 10) according to [24] and subsequently heated to 95 °C for 5 min in the SDS sample buffer [23]. After running the SDS-PAGE, the proteins in the gel were stained with colloidal Coomassie Brilliant Blue G-250 (Roth, Karlsruhe, Germany).

2.3 Production of the Au nanoparticles

The production of the archaeal Au nanoparticles was performed in a two-step procedure. The first step represented Au(III) deposition into the SlaA-ghosts. This was achieved by incubation of 4 mg SlaA-ghosts in 40 ml 3 mM solution of $HAuCl_4$ (pH ~2.5) for 24 hours at room temperature in the dark. The pH of the samples measured after the gold deposition was about 3. In some cases the pH of the gold solution was corrected, prior to the treatment of the SlaA ghosts, to pH 4 by NaOH and after the Au deposition it was slightly changed to pH 3.9. After this first step of Au deposition, the not-deposited Au(III) was removed by centrifugation and subsequent washing of the SlaA-ghost's pellet with triple-distilled water. The amount of not bound gold in the supernatants was determined by using Inductively Coupled Plasma - Mass Spectrometry (ICP-MS) using an Elan 9000 system (Perkin Elmer, USA). The second step, namely the reduction of Au(III) to Au(0) was performed by using 22 mM dimethylaminoboran hydride (DMAB, Merck, Germany) with a pH of 9. At this pH the SlaA-layer starts to dissociate in monomers [22]. However, at pH of 8.5, which is relevant to the samples treated with DMAB, partial disintegration and collapse of the SlaA ghosts occurs [25]. After the addition of DMAB, the solution was centrifuged at 9.000 g for 20 min. One part of the pellet was used for XPS analysis (see below) and the rest of the archaeal bio-Au was dried under vacuum at 35 °C.

Parallel samples of bacterial bio-Au were prepared by using the S-layer sheets of *B. sphaericus* JG-A12 according to [12]. The size and the magnetic properties of the bacterial bio-Au were compared to those of the archaeal bio-Au.

2.4 HR- TEM combined with EDX

In order to ensure the disruption of the SlaA-ghosts into SlaA-layer sheets sonication for 10 s on ice in continuous duty cycle at 100 W was performed using Branson W-250D Ultrasonifier. Both the archaeal and bacterial Au nanoparticles were dehydrated with ethanol and deposited on a carbon coated copper TEM grid. TEM analyses were performed in a high resolution Philips CM 200 transmission electron microscope at an acceleration voltage of 200 kV. Energy dispersive X-ray spectroscopic (EDX) analysis, which provides information about the elemental surrounding of the Au(0), was performed at the same voltage using a spot size of 7 nm and a live counting time of 200 s.

2.5 X-ray Photoelectron Spectroscopy (XPS)

For the XPS analysis, one part of the pellet of the DMAB treated SlaA-ghosts, containing Au(0) nanoparticles, was sonicated and resuspended in triple distilled water.

About 10 µl of the archaeal bio-Au suspension was spread twice over Si-wafers and subsequently dried up. XPS measurements were performed using a scanning auger electron spectrometer (Microlab 310F, Fisions instruments) with field-emission cathode and hemispherical sector analyzer with accessory XPS-unit (Al/Mg - X-ray tube). The X-ray spot had a size of about 2 x 3 mm². Measurements were conducted in CAE mode using pass energy of 10 eV. The carbon 1s peak (284.6 eV) was used for energy calibration.

2.6 SQUID Magnetization Measurements

Magnetization measurements were performed using a Superconducting Quantum Interference Device (SQUID) magnetometer. This instrument allows for measuring the total magnetic moment of a sample, including all atomic and molecular magnetic contributions. Small parts of the prepared archaeal and bacterial bio-Au were fixed in a specially designed sample holder which allows for canceling background contributions to the total magnetic moment. During the measurements, the magnetic field was held constant ($B_0 = 2\,T$) in the superconducting magnetic field coil while the samples were consistently moved through a pick-up coil system of the flux transformer connected to the SQUID. Magnetization data were taken at temperatures $1.8\,K \leq T \leq 300\,K$ using a liquid-He cooled variable-temperature insert installed in the commercial SQUID-magnetometer set up (MPMS, Quantum Design, Inc., San Diego, CA, USA). In order to scale the measured magnetic moments to the amount of substance, the weight of the sample was determined. For calculating the magnetic moment arising from each single gold atom, the proportion of gold in the sample was additionally calculated on the basis of ICP-MS data. All samples studied were checked for iron impurities which could skew magnetic results. The amount of iron determined by ICP-MS was in each sample below the detection limit confirming that iron impurities are not contributing to the measured magnetic signal.

2.7 X-ray Magnetic Circular Dichroism (XMCD)

To unravel the microscopic origin of the archaeal Au nanoparticles magnetism we have performed XMCD measurements at the $L_{2,3}$-absorption edges of gold. This technique is inherently element- and shell-selective, i.e. when the XMCD spectra are recorded at the $L_{2,3}$ edges (2p to 5d transitions) it probes the magnetic polarization of the 5d electronic states of the Au atoms only. The XMCD experiments were performed at the ID12 beam line of the European Synchrotron Radiation Facility (ERSF) in Grenoble. The capsule containing a pressed collection of archaeal Au nanoparticles was attached to the cold finger of a liquid He constant flow cryostat which was inserted in a 17 T superconducting magnet from Cryogenics Ltd..

Circular polarized X-rays generated by an APPLE-II type undulator were monochromatized by a fixed-exit double crystal monochromator equipped with a pair of Si<111>crystals. The circular polarization rate was estimated to be in excess of 95%. The X-ray absorption (XAS) spectra were measured in back scattering geometry using total fluorescence detection mode. The XMCD spectra were obtained by a direct difference of the XAS spectra recorded with opposite helicities while a magnetic field of 17 Tesla was applied along the incident X-ray beam direction. The temperature of the sample was 2.2 K. To make sure that the XMCD spectra are free of experimental artifacts, the measurements were repeated for the opposite direction of the magnetic field.

3. Results and discussion

3.1 Properties of the purified SlaA-layer ghosts

As evident from the results presented in Fig. 1, no intact cells were present in the purified fraction of the SlaA-layer ghosts. The latter (Fig. 1B) possess the shape and the size of the intact cells (Fig. 1A) but are translucent which indicates that they are free of cellular compounds. The SDS-PAGE analysis
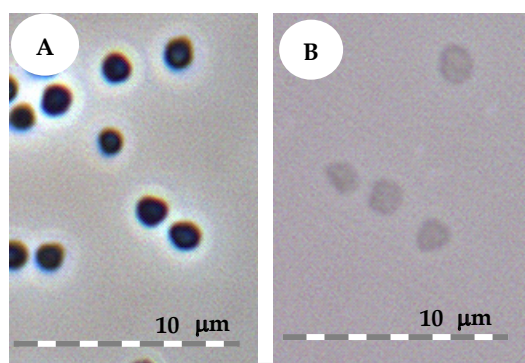

Figure 1. Light microscopic pictures of A) intact cells of *S. acidocaldarius* and B) of the SlaA-ghosts.
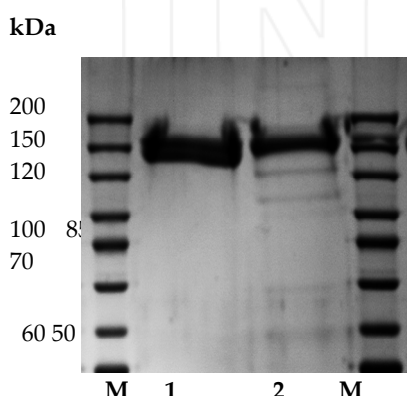

Figure 2. SDS-PAGE protein gel stained with colloidal Coomassie Brilliant Blue G-250: 1) 15 µg of the SlaA-layer ghosts after final purification step with hot SDS; 2) 10 µg of the partially purified SlaA-ghosts, before the final purification step, containing also some other proteins; M) protein marker PageRuler™ #SM0661 (Fermentas GmbH, Germany).

(Fig. 2) clearly demonstrates only one protein band which represents the protein monomers of the denatured SlaA layer. The estimated molecular mass of about 150 kDa is well in line with the molecular weight calculated from the primary structure of the SlaA protein [17].

3.2 Fabrication and characterization of the Au nanoparticles

Bearing in mind that the inside surface of the S-layers facing the cells is negatively charged [21], we assume that the initial deposition of Au(III) occurs inside the SlaA ghosts. The thiol containing cysteine amino acid residues of the SlaA protein of *S. acidocaldarius* are suggested to play an important role for the physico-chemical stability of the protein lattices of this thermoacidophilic archaeon [17,18]. These thiol groups possess, in addition, a strong affinity to Au [26]. In our former work we have demonstrated, however, that the bacterial S-layer of *B. sphaericus* JG-A12, which does not contain thiol groups, can also serve as efficient template for Au-nanoclusters formation [11,12]. Although the underlying mechanisms for the Au(III) binding in both cases are not clear, we expect that in the case of the here studied archaeon the deposition of gold should be more effective owing to the presence of thiol groups present in it.

The ICP-MS measurements of the not bound gold, washed after the deposition, demonstrated that in the case of the bacterial S-layer sheets about 15 % of the initially added gold was deposited onto the S-layer sheets while in the case of the archaeal SlaA ghosts the amount of the deposited gold was only about 6%. One explanation for this at first surprising result could be the fact that in the case of the SlaA-ghosts the gold solution has to be infiltrated into the ghosts through the SlaA-lattice. During this infiltration the Au(III) cations will be caught by the metal-binding ligands of the inner face of the S-layer and deposited there in a way, which we have already described for the deposition of Pd in the whole cells of *B. sphaericus* [4,20]. In the case of the SlaA-ghosts, thiol groups of the cysteine residues certainly contribute to the effective binding and even partial reduction of Au(III). Hence, in the case of the archaeal ghosts, not the whole gold solution but only that part of it which is infiltrated into them is involved in the gold deposition.

After washing of the not bound Au(III) and adding the electron donor (DMAB), the color of the gold/SlaA-ghosts suspension changed from pale yellow to pale purple. This change is based on oscillation changes of conduction band electrons (surface plasmon oscillations) and confirmed the formation of metallic gold nanoparticles [27]. In the case of the bacterial Au nanoparticles, the color change was faster and resulted in dark purple, indicating that a higher amount of gold was reduced. The latter is obviously connected to the immediate reduction

of the gold deposited onto the bacterial S-layer. The SlaA-ghosts loaded with gold interact, however, differently with the DMAB. In addition to the chemical reduction which occurs inside the ghosts, DMAB causes damages of the latter and they start to collapse into imperfect bi-layer structures, containing also some monolayer regions. For this reason, not only the low amount of gold but also the embedding of most of the nanoclusters inside of SlaA-layer sandwiches could be the reason for the observed weaker coloration of the archaeal bio-gold.

3.3 Characterization of the Au nanoparticles

The formed gold nanoparticles were visualized by transmission electron microscopy coupled with EDX. As shown in Fig. 3, the Au nanoparticles were distributed rather irregularly on the bacterial as well as on the SlaA-layer lattices. The recorded EDX spectrum of a spot with SlaA-Au nanoparticles exhibits energy peaks which are specific for gold, as well as for carbon, oxygen, sulfur, and copper (Fig. 3A). The carbon and the copper peaks arise from the carbon-coated copper grid supporting the TEM sample. The elements oxygen and sulfur are structural components of the SlaA protein. The large S peak close to the Au peak suggests that the Au particles

are presumably bound to S of thiol groups of the SlaA protein. This presumption was confirmed by XAS spectra taken at the K - edge of sulfur [28]. The average size of these particles is about 2.5 nm; i.e., a single nanoparticle consists of about 480 Au atoms using the number density of metallic Au, $5.9 \cdot 10^{22}$ atoms/cm^3. However, archaeal Au nanoparticles with substantially smaller and larger sizes were found as well (Fig. 3A). The varying size of the nanoparticles in this case might be partly explained by the collapse of the SlaA ghosts into partly bi-layer structures during the treatment with DMAB. In some cases, two adjacent nanoparticles from the opposite part of the ghosts can then be pressed to each other and aggregate in bigger particles as suggested by others [3]. As mentioned in Materials and Methods, these bi-layer structures were disrupted to monolayer fragments before TEM analyses by sonication. Another explanation for the presence of the bigger Au nanoparticles might be direct reduction of Au(III) onto the monolayer parts of the collapsed SlaA-ghosts. In this case the size of reduced Au nanoparticles is not limited by the shape of the bi-layer sandwiches and they can grow due to the reduction of some remaining Au(III). Interestingly, according to our TEM results, the gold nanoparticles formed on the bacterial S-layer of *B. sphaericus* JG-A12 (Fig. 3B) are bigger, with an average size of about 4 nm. As expected, no sulfur peak is present in the EDX spectrum of the S-layer of *B. sphaericus* due to the absence of cysteine residues in it. The silicon (Si) peak in this spectrum (Fig. 3B) is an artifact coming from the detector. Another difference between the two kinds of gold nanoclusters is that in the case of the archaeal bio-Au all nanoclusters are electron dense, dark spots, while those of the bacterial bio-Au represent a mixture of dark and less dark, semi-translucent nanoclusters. These low dense spots in the case of bacterial bio-Au may possibly represent gold accumulates consisting mainly of unreduced Au(III). This suggestion is in agreement with our results published earlier that in gold nanoparticles formed on S-layer sheets of *B. sphaericus* JG-A12 only about 40% of Au(III) was reduced to Au(0) [11]. The presence of the bigger, electron dense black spots in the case of bacterial bio-Au shown in Fig. 3B could be explained by additional reduction of Au(III) to Au(0) by the electron beam during TEM measurements. Similar electron beam induced reduction of Pd(II) to Pd(0) and Pt(II) to Pt(0) was observed earlier on the bacterial S-layer of *B. sphaericus* [9]. No such translucent particles were found in the TEM pictures of the archaeal bio-gold (Fig. 3A) indicating that all Au nanoparticles in this case have metal structure.
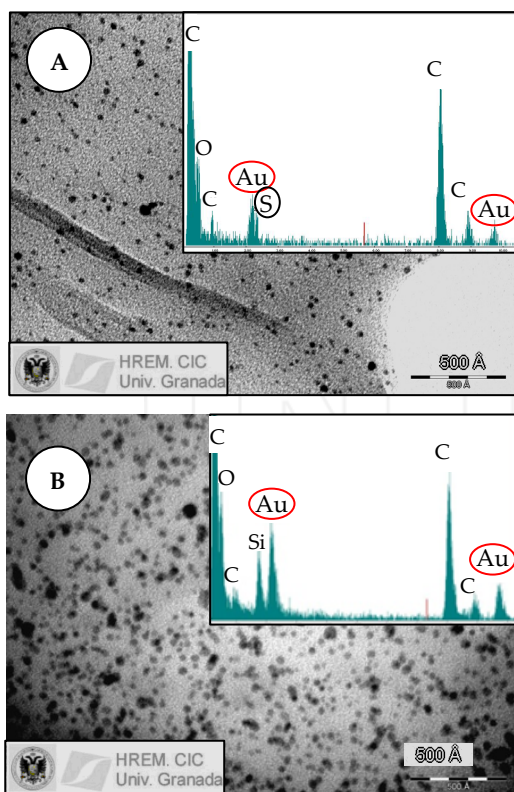

Figure 3. Transmission electron micrographs and representative EDX spectra of gold nanoparticles formed at the: A) SlaA-layer of *S. acidocaldarius;* B) S-layer of *B. sphaericus.*

In order to differentiate the amount of reduced metallic Au(0) in the archaeal bio-Au samples we used X-ray Photoelectron Spectroscopy (XPS).
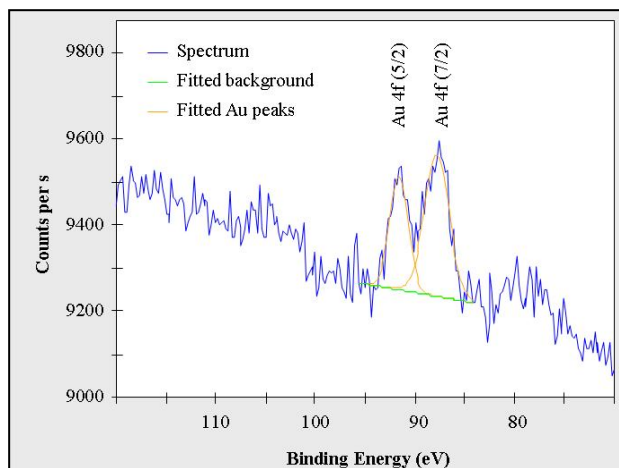
Figure 4. X-ray photoelectron spectrum of the Au nanoparticles at the SlaA layer of *S. acidocaldarius*.

The XPS spectrum presented in Fig. 4 possesses a rather low signal of the gold 4f double peak, due to the small amount of gold on the SlaA-layer. In addition, the signal was shifted by about 4 eV (due to electric charge on the non-metallic sample) to higher energy compared to the spectrum of bulk Au. Nevertheless, the position of the Au 4f (7/2)-peak at about 84 eV (~88 eV in Fig. 4) clearly demonstrates that most of the gold present in the samples is in its metallic state. According to [29], the position of Au 4f (7/2) at 84.0 eV is characteristic for metallic gold, while in Au_2O_3 the position of Au 4f(7/2) is at 85.9 eV, i.e. the latter should be at about 89.9 in our spectrum, but it is not found. The zero-valent oxidation state of gold additionally supports the assumption that the gold–thiol bond does not have the characteristics of gold sulphide and suggest another complexation mode. The obviously complete reduction of Au(III) to Au(0) in the case of archaeal SlaA-ghosts as a template for the nanoclusters fabrication was confirmed by XAS measurements [28]. This result, however, is in contrast to the partial Au(III) reduction occurring on the bacterial S-layer templates. This difference is possibly connected to the slower and perhaps more precise deposition of small amounts of Au(III) onto the gold binding thiol groups of the archaeal ghosts. The latter indicates that the resulting archaeal Au nanoclusters are not only smaller and consisting mostly of Au(0) but that they are also differently organized then those produced on bacterial S-layer sheets.

3.4 Magnetic properties of the Au nanoparticles

The magnetic properties of the formed Au nanoparticles investigated in Dresden by SQUID magnetometry are shown in Fig. 5. As shown in the figure, the two archaeal bio-Au samples reveal a strong magnetic moment which increases according to a Curie-law with decreasing temperature; hence, these Au nanoparticles are paramagnetic. In contrast, the somewhat larger (about 4 nm instead of 2.5 nm) bacterial bio-Au nanoparticles

formed on the thiol-free S-layer of *B. sphaericus* do not show magnetic moments. Possible reasons for the latter observation may be the fact that the bacterial nanoclusters are not fully reduced to Au(0), that they are bigger and that the Au is not bound to thiol groups. In Fig. 5B we show the magnetic moments per Au atom of the two archaeal bio-Au samples calculated from the data of Fig. 5A and the amount of Au in the samples from ICP-MS data. The data show that each Au atom in the cluster carries a mean moment of 0.08 – 0.1 μ_B (assuming that all Au atoms in the cluster contribute equally). The difference of the saturation magnetization, i.e. of the moments of the two samples could be caused by the different pH-values of the Au-solutions used for preparing the samples. In the case of sample 1, the gold solution had a pH of 3.1 and in the case of sample 11 the pH was 3.9. The observed moments are substantially larger than the ones observed for thiol-capped Au nanoclusters [14] and other chemically produced nanoparticles [1].

The results from the XMCD experiments, performed at T = 2.2 K and a field of B=17 T, are depicted in Fig. 6.
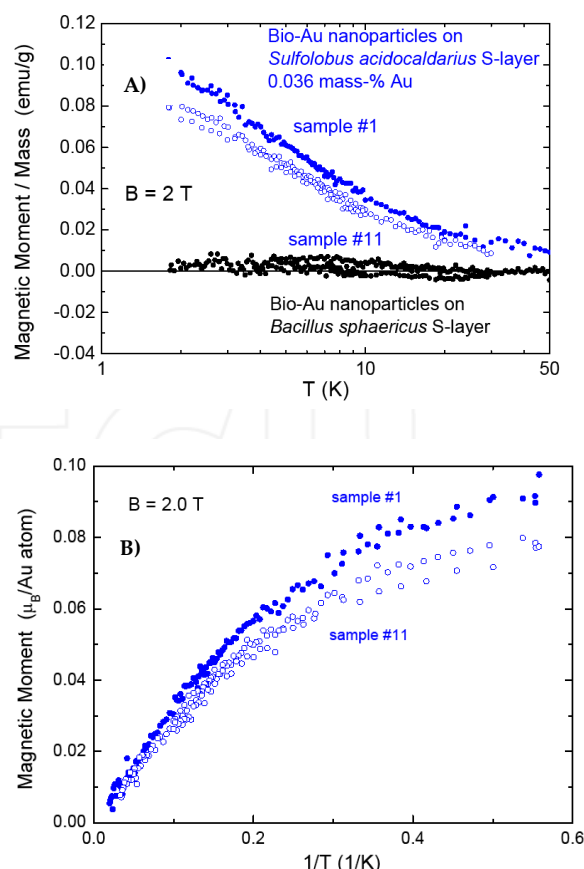

Figure 5. A). Magnetic moment per mass of Au in three bio-Au nanoparticle samples as a function of temperature in a field of B = 2 T; B) Magnetic moment per Au atom in two archeal bio-Au nanoparticles as a function of inverse temperature in a field of B = 2 T.
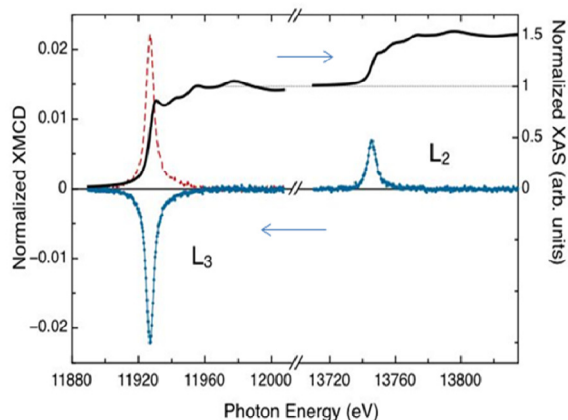
Figure 6. XMCD and XAS spectra at the Au L_3 and L_2 edges, measured at T = 2 K and an applied field B = 17 T. XMCD and XAS are scaled with the same factor so that the L_3 edge jump of the XAS spectra is unity: (—) XAS; (blue …) XMCD data (see experimental section), (red - -) XMCD with the magnetic field applied in the opposite direction.

An excellent signal-to-noise ratio in the spectra allowed to detect the orbital, spin and total magnetic moments of the 5d states of Au using a set of magneto-optical sum rules [30,31]. The number of holes in the 5d band was estimated to be n_h=0.77, from comparison of the $L_{2,3}$-XAS spectra with the ones from the bulk Au metal [28]. This value is substantially larger than the corresponding one for bulk Au (n_h=0.62) [32]. The values obtained for the spin and orbital magnetic moments are averaged over the core and the surface of the particle. The values m_L=0.011(1) μ_B, m_S=0.039(1) μ_B, and m_L/m_S = 0.28(1), were found, yielding the total mean magnetic moment per Au atom, m_{Au} = 0.050(2) μ_B/Au. This value is in good agreement to the mean magnetic moment per Au atom measured for this sample by SQUID magnetometry in Zaragoza [28]. It is up to a factor of two smaller than those of the above mentioned samples investigated by SQUID magnetometry as well. The moment might be different for different batches (see Fig. 5) due to different Au nanoparticles size distributions in them.

There are large differences to the values found in the other two Au nanoparticles studied with XMCD so far, namely Au capped with PAAHC [1] and Au capped with dodecanethiol [33]. The value of the m_L/m_S=0.28(1) ratio is the highest ever found for Au in nanoparticles (m_L/m_S=0.145 or 0.10) [1,33], and m_{Au} is 50 times larger than that found in Au PAAHC capped nanoparticles [1], or nearly 100 times larger than in Au dodecanethiol capped ones [33]. For these samples, the mechanism giving rise to Au magnetism appears to be the increase in the number of holes in the 5d band due to the electron transfer from Au atoms at the surface towards the bound capping atoms. In the present case it is proven in the previous sections, by comparison to the non-magnetic Au on B. *sphaericus* which contains no thiol group, that Au is

bound to the *S*-layer by sulfur of the thiol group of the cysteine amino acid residues in the SlaA proteins. Thus, though the mechanism of magnetic moment induction is similar to the one in Au capped with dodecanethiol case [33], namely Au-S binding, the effectiveness in producing a magnetic moment is extraordinarily larger in the present case of archaeal bio-Au nanoparticles system.

Therefore, we suggest that the magnetic properties of the archaeal gold nanoparticles formed by using the SlaA-ghosts as a template are connected to their full reduction to Au(0), and depend in particular on the transfer of electrons from Au to S to form the binding of Au to thiol groups. Possibly, the size of the formed nanoparticles is important as well. These so-called size and ligand effects determine the electronic band structure and number of holes in the 5*d*-electron band of Au, which in turn influences the magnetic behavior of the formed gold nanoparticles. More details on the magnetic properties of the archaeal bio-Au nanoparticles will be communicated in a forthcoming publication [28].

4. Conclusions

In this study we have demonstrated that the SlaA ghosts of *S. acidocaldarius* serve as a more efficient template for complete reduction of Au(III) to Au(0) than the S-layers of *B. sphaericus*. Moreover, in contrast to the *B. sphaericus* S-layer the SlaA ghosts are an excellent macromolecular template for formation of magnetic Au(0) nanoparticles. The advantages of the SlaA-ghost matrix seem to be related to its unusual shape and biochemical characteristics which are responsible for precise deposition of gold cations. The thiol groups of the SlaA protein are most likely essential for the initial deposition of Au(III) inside the SlaA ghosts, its efficient reduction, and the evocation of the magnetism in the reduced Au(0) nanoparticles.

5. Acknowledgments

6. References

[1] Y . Yamamoto, T. Miura, M. Suzuki, N. Kawamura, H. Miyagawa, T. Nakamura, K. Kobayashi, T. Teranishi, H. Hori, Direct observation of ferro- magnetic spin polarization in Au nanoparticles. *Phys. Rev. Lett.,* vol. 93, pp. 116801-1 – 116801-4, 2004.

[2] S. Zhu, W. Zhou, Optical properties and immunoassay of noble metal nanoparticles. *J. of Nanomaterials*, 2010 doi:10.1155/2010/562035.

[3] P. Zhang, T. K. Sham, X-ray studies of the structure and electronic behavior of alkanethiolate-capped gold nanoparticles: The interplay of size and surface effects. *Phys. Rev. Lett.*, vol. 90, pp.245502-1-245502-4, 2003.

[4] N. Creamer, I. Mikheenko, P. Yong, K. Deplanche, D. Sanyahumbi, J. Wood, K. Pollmann, M. Merroun, S. Selenska-Pobell, L. E. Macaskie, Novel supported Pd hydrogenation bionanocatalyst for hybrid homo- geneous/heterogeneous catalysis. *Catalysis Today,* vol. 128, pp. 80-87 (2007).

[5] R. Narayanan, Recent advances in noble metal nanocatalysts for suzuki and heck cross-coupling reactions. *Molecules,* vol. 15, pp. 2124-2134, 2010.

[6] S.B. Lee, Focus on nanoparticles for cancer diagnosis and therapeutics. *Nanomedicine,* vol. 2, pp. 647-648, 2007.

[7] A. J. Haes, S.L. Zou, G. C. Schatz, R.P. Van Duyne, A nanoscale optical biosensor: The long range distance dependence of the localized surface plasmon resonance of noble metal nanoparticles. *J. Phys. Chem.,* vol. 108, pp. 6961-6968, 2004.

[8] Y.J. Kim, R.C. Johnson, J.T. Hupp, Gold nanoparticle- based sensing of "spectroscopically silent" heavy metal ions. *Nano Let.,*. vol. 1, pp. 165-167, 2001.

[9] R. Wahl, M. Mertig, J. Raff, S. Selenska-Pobell, W. Pompe, Electron-beam induced formation of highly ordered Pd and Pt nanoparticle arrays on the S-layer of *Bacillus sphaericus* NCTC9602. *Advanced Materials,* vol. 13, pp. 736-740, 2001.

[10] K. Fahmy, M. Merroun, K. Pollmann, J. Raff, O. Savchuk, C. Hennig, S. Selenska-Pobell, Secondary structure and Pd(II) coordination on S-layer proteins from *Bacillus sphaericus* studied by infrared and X-ray absorption spectroscopy. *Biophysical Journal*, vol. 91, pp. 996-1007, 2006.

[11] M. Merroun, A. Rossberg, C. Hennig, A.C. Scheinost, S. Selenska-Pobell, Spectroscopic characterization of gold nanoparticles formed by cells and S-layer proteins of *Bacillus sphaericus* JG-A12. *Material Science and Engineering*, vol. 27, pp. 188-192, 2007.

[12] U. Jankovski, M. Merroun, S. Selenska-Pobell, K. Fahmy, S-layer protein of *Lysinibacillus sphaericus* JG-A12 as matrix for Au(III) sorption and nanoparticles formation. *Spectroscopy*, vol. 24, pp. 177-181, 2010.

[13] T. Herrmannsdörfer, A.D. Bianchi, T.P. Papageorgiou, F. Pobell, J. Wosnitza, K. Pollmann, M. Merroun, J. Raff, S. Selenska-Pobell, Magnetic properties of transition-metal nanoclusters on a biological substrate. *J. of Magnetism and Magnetic Materials,* vol. 310, pp. E821-E823, 2007.

[14] P. Crespo, R. Litran, T.C. Rojas, M. Multigner, J.M. de la Fuente, J.C. Sanchez-Lopez, M.A. Garcia, A. Hernando, S. Penades, A. Fernandez, Permanent magnetism, magnetic anisotropy, and hysteresis of thiol-capped gold nanoparticles. *Phys. Rev. Lett.,* vol. 93, pp. 087204-1 – 087204-4, 2004.

[15] S. Dieluweit, D. Pum, U.B. Sleytr, Formation of a gold superlattice on an S-layer with square lattice symmetry. *Supramolecular Science,* vol. 5, pp. 15-19, 1998.

[16] A. Veith, A. Klingl, B. Zolghadr, K. Lauber, R. Mentele, F. Lottspeich, R. Rachel, S.V. Albers, A. Kletzin, *Acidianus,* *Sulfolobus* and *Metallosphaera* S- layers: Structure, composition and gene expression. *Molecular Microbiology,* vol. 73, pp. 58-72, 2009.

[17] H. König, R. Rachel, H. Claus, Proteinaceous surface layers of archaea. In: *Archaea: Molecular and Cellular Biology*, ASM Press, Herndon, pp. 315-353, 2007.

[18] H. Engelhardt, Are S-layers exoskeletons? The basic function of protein surface layers revisited. *J. of Structural Biology,* vol. 160, pp. 115-124, 2007.

[19] S. S.Mark, M.Bergkvist, X.Yang, L.M. Teixeira, P.Bhatnagar, E.R. Angert, C.A. Batt, Bionano- fabrication of metallic and semiconductor nanoparticle arrays using S-layer protein lattices with different lateral spacings and geometries. *Langmuir,* vol. 22, pp. 3763-3774, 2006.

[20] S. Selenska-Pobell, M. L. Merroun, Accumulation of heavy metals by microorganisms: Bio- mineralization and nanocluster formation. In: *Prokaryotic Cell Wall Components - Structure and Biochemistry*, Springer Verlag, Heidelberg, pp. 483- 500, 2010.

[21] D. Pum, M. Sara, U.B. Sleytr, Structure, surface charge, and self-assembly of the S-layer lattice from *Bacillus coagulans* E38-66. *J. of Bacteriology,* vol. 171, pp. 5296-5303, 1989.

[22] H. Michel, D. Neugebauer, D. Oesterhelt, The 2-D crystalline cell wall of *Sulfolobus acidocaldarius*: Structure, solubilization, and reassembly. In: *Electron Microscopy at Molecular Dimensions*, pp. 27-35, 1980.

[23] U.K. Laemmli, Cleavage of structural proteins during assembly of head of bacteriophage-T4. *Nature,* vol. 227, pp. 680-685, 1970.

[24] D.W. Grogan, Isolation and fractionation of cell envelope from the extreme thermo-acidophile *Sulfolobus acidocaldarius*. *J. of Microbiological Methods,* vol. 26, pp. 35-46,1996.

[25] T. Reitz, PhD-Thesis, Univ. Freiberg, Germany, 2011.

[26] S.-U. Kim, J.-H. Lee, T. Lee, J. Min, J.-W. Choi, Nanoscale film formation of recombinant azurin variants with various cysteine residues on gold substrate for bioelectronic devices. *J. Nanosci. Nanotechnol.*, vol. 10, pp. 3241-3245, 2010.

[27] P. Mulvaney, Surface plasmon spectroscopy of nano-sized metal particles. *Langmuir,* vol.12, pp.788-800, 1996.

[28] J. Bartolomé, F. Bartolomé, L. M. Garcia, A.I. Figueroa, A. Repolles, M. J. Martínez-Pérez, F. Luis, F. Wilhelm, A. Rogalev, R. Schönemann, T. Herrmannsdörfer, T. Reitz, M. Merrroun, A. Geissler, S. Selenska-Pobell, Large magnetic moment of bio- Au nanoparticles on archeal S-layer ghosts (to be published).

[29] K. Juodkazis, J. Juodkazyte, V. Jasulaitiene, A. Lukinskas, B. Sebeka, XPS studies on the gold oxide surface layer formation. *Electrochemistry Communications*, vol. 2, pp 503- 507, 2000.

[30] B. T. Thole, P. Carra, F. Sette, G. van der Laan, X-ray circular dichroism as a probe of orbital magnetization *Phys. Rev. Lett.*, vol. 68, pp. 1943- 1946, 1992.

[31] P. Carra, B.T. Tolle, M. Altarelli, X.-D. Wang, X-ray circular dichroism and local magnetic fields. *Phys. Rev. Lett.*, vol. 70, pp. 694-697, 1993.

[32] A. Rogalev, F. Wilhelm, N. Jaouen, J. Goulon, J-P. Kappler, X-Ray Magnetic Circular Dichroism: Historical Perspective and Recent Highlights. *Lecture Notes in Physics,* vol. 697, pp. 71-93, 2006.

[33] J.S. Garatonaindia, M. Insausti, E. Goikolea, M. Suzuki, J.D. Cashion, N. Kawamura, H. Ohsawa, I. Gil de Muro, K. Suzuki, F. Plazaola, T. Rojo, Chemically induced permanent magnetism in Au, Ag and Cu nanoparticles: localization of the magnetism by element selective techniques. *Nano Letters,* vol. 8, pp.661-667, 2008.